RSC Advances

PAPER

View Article Online
View Journal | View Issue

Cite this: *RSC Adv.*, 2022, **12**, 21297

Fabrication of a graphene-based sensor to detect the humidity and the temperature of a metal body with imprecise data analysis

Usama Afzal, *[ad] Muhammad Aslam, [b] Fatima Afzal,[c] Kanza Maryam,[c] Naveed Ahmad,[d] Qayyum Zafar [e] and Zahid Farooq[f]

Graphene is a 2D material with remarkable properties. The present study demonstrates the fabrication of a graphene-based sensor for measuring the temperature and humidity of a metal body. The graphene sensor was fabricated by depositing a thin film of graphene nanoparticles between silver electrodes (separated by ~50 μm) on a glass substrate. The graphene thin film was characterized by XRD, Raman spectroscopy and UV-vis techniques. The capacitance and resistance for both the relative humidity (in the range of 0–100% RH) and temperature (in the range of 230–310 K) were measured using an LCR meter at 1 kHz in a controlled chamber. The graphene-based sensor expressed high sensitivity with fast response and recovery times for both humidity and temperature with long stability and low hysteresis curves. The sensor was also tested on a metal body, which expressed a good response time. Moreover, the measured data of capacitance and resistance was analyzed with classical and neutrosophic analysis as an application of modern material statistics. It was observed that neutrosophic analysis is more flexible for analyzing the capacitance and resistance of the fabricated sensor.

Received 4th June 2022
Accepted 12th July 2022

DOI: 10.1039/d2ra03474c

rsc.li/rsc-advances

1. Introduction

Studies on microelectronics and nanotechnology are on the rise and researchers have been working on flexible circuits as well as devices. Many nanomaterials have been used for this purpose, such as carbon-containing materials, *i.e.*, carbon nanofibers (CNFs)[1] and carbon nanotubes (CNTs).[2,3] Graphene is one of the well-known carbon-containing materials. It is a zero-bandgap[4] allotropic form of carbon having a two-dimensional hexagonal lattice structure. Graphene is more advantageous than other materials such as graphite due to its mechanical properties (since it may be single-layered or multilayered[5]), thermal conductivity (graphene has very high thermal properties) of about 5000 W m^{-1} K (ref. 6), electric conductivity (about 10^4 to 10^5 S m^{-1} for pure graphene[7]) and large surface area.[8] Researchers have also used the oxide form of graphene which is produced through different methods. The Hummers' method is one of the commonly known methods, which is used by different researchers in their work as explained in the following ref. 9–12. Due to the remarkable properties of graphene, it has been used in the fabrication of different devices such as sensors,[13] solar cells[14] and others. For example, a humidity sensor based on the thin films of graphene oxide with thermal annealing at the temperature of 1200 °C was proposed.[15] A highly sensitive humidity graphene oxide was also fabricated with evenly dispersed multi-walled carbon nanotubes.[16] Similarly, a wearable temperature sensor based on graphene nanowalls was proposed.[17] For further examples, the reader may be interested in the following ref. 16, 18–26. From the above-mentioned references, it was observed that the data measured (whether resistance or capacitance) were analyzed through classical graphs and tables, which are based on the fixed-point values, *i.e.*, fixed values of capacitance and resistance at a specific point of humidity and temperature. However, if someone measures data in the interval, classical methods do not analyze the data well. This is why we should move on to some novel statistics approaches, such as the neutrosophic approach, *etc.*

A neutrosophic approach is used for the analysis of the data variance, as proposed by Smarandache.[27] It is a flexible and reliable technique of statistics, which has numerous advantages over the classical approach. The neutrosophic approach uses interval data for the analysis,[28] which is its biggest advantage because classical analysis is only specified around the fixed-

[a]*Visiting Lecturer, Faculty of Science, Gift College, Hafizabad 52110, Pakistan. E-mail: mohammadusamafzal7@gmail.com*

[b]*Department of Statistics, Faculty of Science, King Abdulaziz University, Jeddah 21551, Saudi Arabia. E-mail: aslam_ravian@hotmail.com*

[c]*Bachelor Student, School of Chemistry, University of the Punjab, Lahore 54000, Pakistan. E-mail: f.afzal.edu@gmail.com; k.maryam.edu@gmail.com*

[d]*Department of Physics, University of Education, Township Campus, Lahore 54000, Pakistan. E-mail: dr.naveedahmadsammar@ue.edu.pk*

[e]*Department of Physics, University of Management and Technology, Lahore 54000, Pakistan. E-mail: qayyumzafar@gmail.com*

[f]*Department of Physics, University of Education, Faisalabad Campus, Pakistan. E-mail: Zahid.farooq@ue.edu.pk*

point or determined data. This is why the use of this approach has gained importance for the variance analysis of different problems in several fields, *e.g.* medicine,[29] applied sciences,[30] astrophysics[31] and material statistics like resistance and capacitance analysis,[32–34] *etc.* Moreover, the neutrosophic technique is more helpful than classical techniques; see the following references for examples.[35–37] Different statistical techniques have been developed under neutrosophic statistics by Muhammad Aslam.[38,39]

Herein, we report the fabrication of a graphene-based sensor for measuring the humidity and temperature effects of the metal body. A thin film of graphene nanoparticles was deposited on a glass substrate between two silver electrodes whose capacitance and resistance with respect to temperature and relative humidity were measured at 1 kHz with an LCR meter. The data were analyzed through classical and neutrosophic approaches (a similar analysis was performed for the interval data of the humidity sensor based on methyl green[40]). Through this work, we have tried to develop an application of material statistics (a study in which data regarding material properties are analyzed through different methods of statistics) for the said graphene sensor's imprecise data based on modern statistics methods.

2. Experimental

Graphene with 99.9% purity has been used in this experiment. For the fabrication of the sensor, the glass substrate (25 × 25 mm) was cleaned with ethanol (for 15 minutes) and then dried with the help of a nitrogen gun. Silver electrodes (separated about 50 μm) were deposited on the substrate by thermal evaporation with a shadow mask at 10^{-5} mbar pressure. After this, a solution of graphene nanoparticles was prepared by taking about 40 mg graphene and 1.6 ml naphtha. The solution was stirred for five hours and then filtered. About 50 μl of the solution was deposited between the electrodes through a micropipette. In the end, our fabricated sensor (of dimension 25 × 25 mm) was ready for characterization having a 2 μm thickness of the thin film of graphene nanoparticles with an 8 mm × 25 mm surface area as shown in Fig. 1. The whole process was performed at room temperature, *i.e.* 20 °C.

Fig. 1 Schematic diagram of the sample.

The structure of the graphene nanoparticle thin film was characterized by X-ray diffraction (XRD), the optical properties of the sample were studied by the UV-vis technique and the quality of the thin film was investigated by Raman spectroscopy. The electrical study was performed in the laboratory using an AT2816B LCR meter at 10 kHz, which was associated with a controlled chamber. This controlled chamber contained a heater to increase the temperature of the chamber and a humidifier to produce humidity inside the chamber. The characterization setup is shown in Fig. 2. First, we measured the variances in capacitance and resistance with respect to changes in temperature (from 230 to 310 K). After this, we measured the capacitance and resistance variance with respect to changes in the relative humidity inside the chamber (from 0 to 90% RH). All the data were collected at intervals, with both maximum and minimum value changes in capacitance and resistance at a specific point of relative humidity, as well as temperature. Also, the sample has shown high sensitivity with high response and recovery times for both relative humidity (% RH) and temperature (K). We repeated the whole experiment several times but found very minor variations (about 1 to 1.5%, which can be neglected).

3. Results and discussion

The structure of the graphene thin film has been studied by the XRD technique, as shown in Fig. 3. The following pattern was ben observed in the range 5° < 2° theta < 70°. The pattern satisfies the standard value. There is a sharp peak, *i.e.* (002), at about 25°, which expresses the (002) plane with a *d*-spacing of 3.562 Å based on Bragg's law and also provides information about the size of the lattice constant, *i.e.*, 2.46 Å.[41]

Fig. 4(a) shows the UV-vis spectrum of the graphene thin film. The peak of the spectrum is found at 280 nm, which indicates that the thin film is a good absorber of UV-C light. The

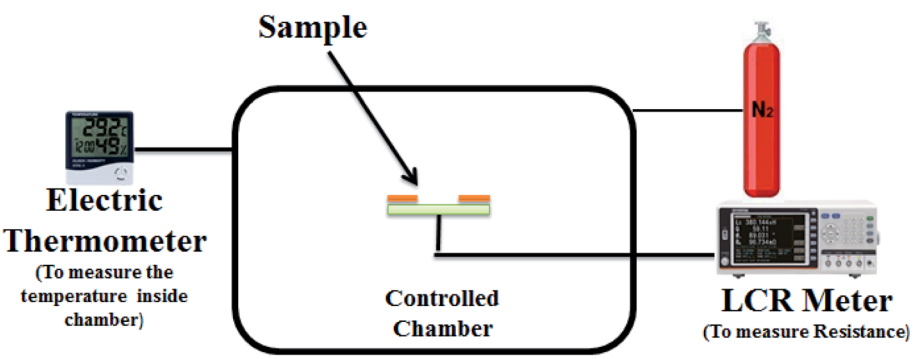

Fig. 2 Characterization setup used in the experiment.

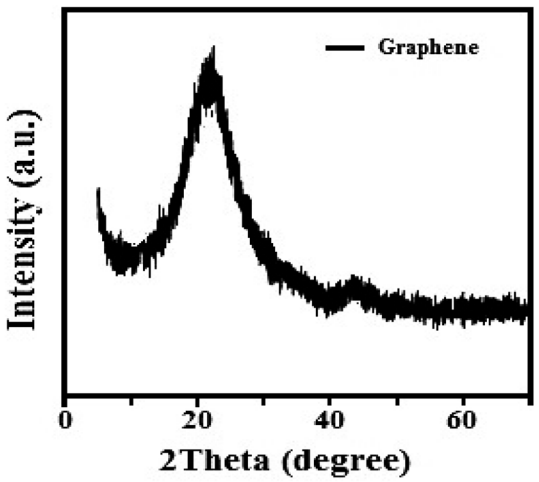

Fig. 3 XRD pattern of the graphene nanoparticles-based thin film.

absorption efficiency indicates that it can be used in light sensing, photodiodes, or solar cell applications. Also, Fig. 4(b) shows the Raman spectrum. We observed three peaks as D, G and 2D at about 1376, 1649 and 2725 cm^{-1}, respectively. 'D' is a defect peak, which highlights the defects as well as disorders between layers of graphene. 'G' is the characteristic peak of the carbon structure sp^2, which highlights the symmetry as well as the crystallization of the graphene structure. '2D' is a double-phonon-resonance peak, which expresses the graphene stacking degree, *i.e.*, indicating the presence of graphene.[42,43]

We investigated the electric properties of the sample for humidity and temperature sensing, which were measured in the lab as shown in Tables 1 and 2 for humidity and temperature sensors, respectively. We measured the interval values of capacitance and resistance because we wanted to observe the whole variance of the sensor's capacitance and resistance (*i.e.*, the minimum change value and maximum change value as in our previous work[3]) at a specific value of temperature and relative humidity.

Table 1 The capacitance and resistance of the graphene nanoparticles thin film as a humidity sensor

Relative humidity (% RH)	Capacitance (pF)	Resistance (kΩ)
0	[2.345, 2.923]	[36.024, 36.820]
10	[2.421, 3.213]	[35.122, 35.422]
20	[2.710, 3.312]	[33.245, 33.945]
30	[3.001, 3.299]	[31.108, 31.708]
40	[3.398, 3.663]	[28.378, 28.930]
50	[3.419, 3.824]	[26.378, 26.991]
60	[3.721, 4.143]	[24.524, 25.321]
70	[3.921, 4.521]	[23.216, 23.879]
80	[4.007, 4.791]	[23.116, 23.290]
90	[4.172, 4.810]	[23.102, 23.208]
100	[4.671, 4.957]	[23.079, 23.102]

Table 2 The capacitance and resistance of the graphene nanoparticles thin film as a temperature sensor

Temperature (K)	Capacitance (μF)	Resistance (Ω)
230	[10.01, 11.12]	[90, 111]
240	[10.21, 10.63]	[94, 98]
250	[8.62, 9.71]	[103, 116]
260	[7.52, 8.55]	[117, 133]
270	[6.29, 7.58]	[132, 159]
280	[4.72, 5.18]	[193, 212]
290	[4.02, 4.49]	[223, 249]
300	[3.32, 3.70]	[270, 301]
310	[2.56, 2.97]	[337, 390]

3.1. The effect of humidity on the capacitance and resistance of the sample

It can be seen from Table 1 that the capacitance of the humidity sensors increased. Initially, the sensors showed a small variation in capacitance; however, the capacitance increased sharply as the humidity in the air in the chamber increased. This is because initially, there were several immobile layers of sensing thin films but as the humidity of the air in the chamber increased and was

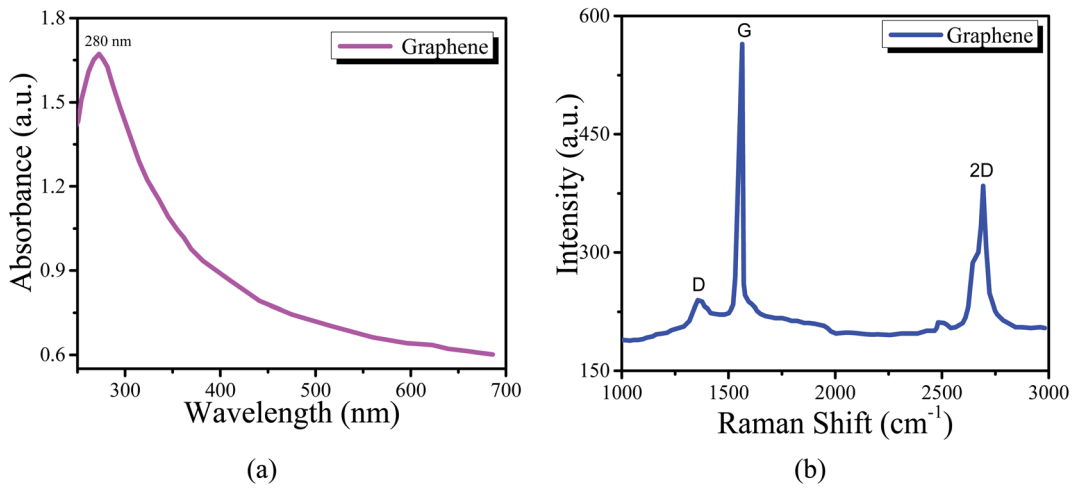

Fig. 4 (a) UV-vis spectrum of the graphene nanoclusters thin film. (b) Raman spectrum of the graphene nanoclusters thin film.

absorbed by the films, the immobile layers were converted into mobile layers.[44] This means that the capacitance of the humidity sensors is directly proportional to the absorption of humidity. If 'ε_d' is the dielectrics permittivity of the sensing thin films with 'ε_0' as the vacuum permittivity and 'd' is the distance between the electrodes and 'A' is the area of electrodes, the capacitance for the humidity sensors is written as follows:

$$C_{(\%\ \mathrm{RH})} = \frac{A\varepsilon_d\varepsilon_0}{d} \quad (1)$$

Since the capacitance changes with the changes in the humidity of the air, it can be defined by some factors like the surface morphology of the sensing film, the polarizability of the material, the dielectric constant of the water and material and electrode distance. Dielectric permittivity is an important factor that can cause capacitance to increase. The relative permittivity of water is very high (*i.e.*, 80), which is significantly higher than the relative permittivity of organic semiconductors.[45] This high relative permittivity of water increases the dielectric permittivity of the sensing film; therefore, the relationship between the capacitance and the dielectric constant under dry and humid conditions can be written as follows:[46]

$$\frac{C_h}{C_d} = \left(\frac{\varepsilon_h}{\varepsilon_d}\right)^n \quad (2)$$

In eqn (2), 'ε_h' is the humid dielectric constant, 'ε_d' is the dry dielectric constant, 'C_h' is the humid capacitance and 'C_d' is the dry capacitance with 'n' being the morphology element of the dielectric. The absorption of humidity on films can also be observed with weak hydrogen bonding and van der Waals interactions of humidity with sensing films.[47] If an external electric field acts on the water molecules and the molecules become polarized, it can be written as follows:

$$P = \alpha E \quad (3)$$

In eqn (3) above, 'P' is the polarity, 'α' is the polarizability and 'E' is the external field. Moreover, it was observed that the polarizability of the thin films is directly proportional to the dielectric constant.[48] This polarization may have an electronic nature, dipolar nature or ionic nature.[49] If 'ε_0' represents the free space permittivity and 'ε_d' represents the relative permittivity, the relation between polarization and dielectric constant by using the Clausius Mossotti equation[50] is as follows:

$$\frac{\varepsilon_d - 1}{\varepsilon_d + 2} = \frac{N_d\alpha_d}{3\varepsilon_0} \quad (4)$$

From eqn (4), we can write a simulation equation for the capacitance of sensors[51] as follows:

$$\frac{C_h}{C_d} = \frac{[1 + 2N_d\alpha_d(1 + kH)]}{3\varepsilon_0} \Big/ \frac{[1 - N_d\alpha_d(1 + kH)]\varepsilon_d}{3\varepsilon_0} \quad (5)$$

Here 'k' is known as the capacitive humidity factor, which is 1.6×10^{-2} $(\mathrm{RH})^{-1}$, and 'H' is the relative humidity level.

Table 1 shows the resistance variance of the humidity sensors. The resistance decreased as the humid air level increased in the chamber. Initially, the sensors showed high variation but as the humidity increased, the variation became small. The change in the resistance of the sensors is related to the absorption of humidity on the sensing films. As the sensing films absorb humidity, this humidity becomes a reason for an increase in charge carriers, *i.e.*, water molecules also work as dopants (because the molecules of water interact with the atoms/molecules of graphene and provide a path to pass the electric charge from the graphene). Also, it is seen that the absorption of humidity may lead to the dissociation of ions. These ions increase the conductivity of the sensing film and the resistance starts to decrease because both are inversely proportional to each other.[52] If 'A' is the area of sensing films, 'l' is the length and 'α' is the conductivity of sensing films, then resistance for sensors can be written as

$$R = \frac{lA}{\alpha} \quad (6)$$

From eqn (6), it is clear that the resistance depends on the absorption rate of the films, length of films, conductivity, and the area of films.

3.2. The effects of temperature on the capacitance and resistance of the sample

Table 2 shows the effects of temperature on the capacitance and resistance of the sample. It is seen that first resistance starts to decrease till 245 K because graphene also has conductive properties[53,54] but then it gradually starts to increase. This shows that the thin film of graphene nanoparticles is a good conductor at room temperature. However, as the temperature starts to rise, then the air (present in the chamber) starts to expand in the nanoparticle layers, which becomes a reason for thermal distribution.[55] Due to the thermal distribution, the thermal expansion between the layers of nanoparticles increases and contact between layers decreases. This phenomenon leads to a decrease in the tunnel area. As the tunneling effects become weaker, then resistance starts to increase. From eqn (6), the temperature increased and the conductivity decreased due to the change in atomic motion of the sensing layer and electrodes, hence the resistance of the sample increased but the capacitance decreased. There is an inverse relationship between resistance and capacitance (for LCR[40]) as follows:

$$R\ \alpha\ \frac{1}{C} \quad (7)$$

Here, 'R' is the resistance and 'C' is the capacitance at the constant frequency of 1 kHz.

3.3. Sensitivity with response and recovery time

Sensitivity can be defined as "a tiny variation in measuring, sensor signal to premier sensor signal".[56] The formula for finding sensitivity is written as follows:

Table 3 Comparison of sensitivity, response and recovery time of humidity and temperature sensors

Sensors	Frequency	Band gap	Sensitivity (%)		Response time	Recovery time
			Capacitance	Resistance		
Humidity	1 kHz	0–100% RH	2.612 (pF/% RH)	12.927 (kΩ/% RH)	1.60 s	2.15 s
Temperature	1 kHz	230–310 K	8.8 (μF/K)	375 (Ω/K)	3 s	8.1 s

Table 4 Comparison of the present work with previously published research work for humidity sensors

Nano-materials	Band gap	Sensitivity	Response time	Recovery time
SnO_2 (ref. 57)	30–85% RH	2–33 pF/RH%	120–170 s	20–60 s
Multi-wall carbon nanotubes[58]	11–97% RH	0.026 pF/% RH	45 s	15 s
Methyl green[40]	40–80% RH	(122.37 pF/% RH) & (31 KΩ/% RH)	200 s	60 s
Methyl red[59]	30–95% RH	(16.92 pF/% RH) & (0.307 MΩ/% RH)	10 s	10 s
Graphene nanoparticles (present study)	0–100% RH	(2.612 pF/% RH) & (12.927 kΩ/% RH)	1.60 s	2.15 s

Table 5 Comparison of the present work with previously published research work for temperature sensors

Nano-materials	Band gap	Sensitivity	Response time	Recovery time
CNTs on PET[60]	40–100 °C	0.4% °C	300 ms	4 s
Graphene on PDMS[61]	30–100 °C	2.11% K	3 s	20 s
rGO on PET[62]	30–100 °C	0.6345% °C	1.2 s	—
rGO on PI[63]	25–45 °C	1.30% °C	0.443 s	0.330 s
Graphene nanoparticles (present study)	230–310 K	(8.8 μF/K) & 375 (Ω/K)	3 s	8.1 s

$$S = \left| \frac{R_{max}/C_{max} - R_{min}/C_{min}}{T_{max}/RH_{max} - T_{min}/RH_{min}} \times 100 \right|$$

- 'C_{max}' and 'R_{max}' are the maximum measured values of capacitance and resistance, respectively.
- 'C_{min}' and 'R_{min}' are the minimum measured values of capacitance and resistance, respectively.
- 'T_{max}' and 'RH_{max}' are the maximum measured values of temperature and relative humidity, respectively.
- 'T_{min}' and 'RH_{min}' are the minimum measured values of temperature and relative humidity, respectively.

The sensitivities of the samples for both humidity and temperature sensors are shown in Table 3. Comparisons of the present work with previous work can be seen in Tables 4 and 5 for humidity and temperature, respectively.

3.4. Hysteresis curves and long stability for humidity and temperature

Hysteresis curves of the graphene sensor for the humidity and temperature have been studied by calculating the calibration

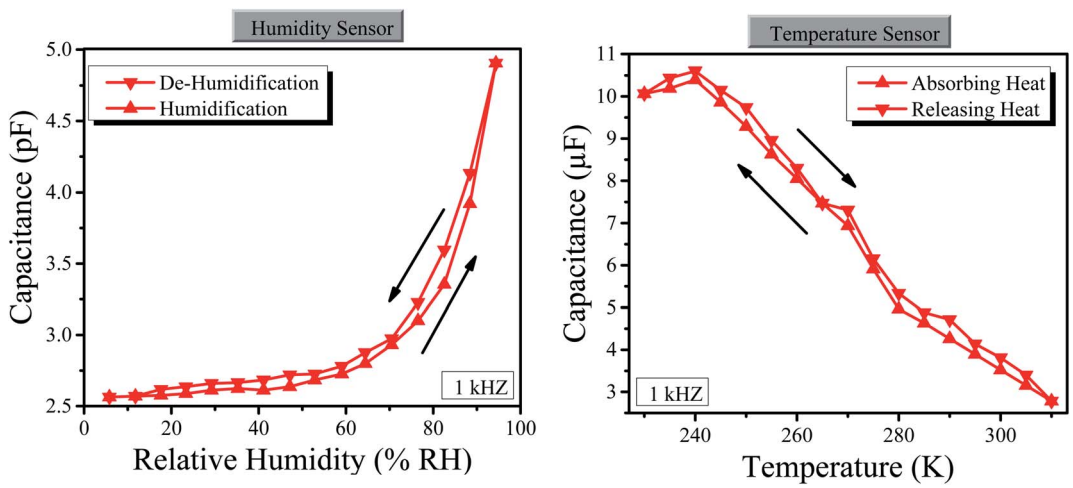

Fig. 5 (Left) Hysteresis curves of the humidity sensor. (Right) Hysteresis curves of the temperature sensor.

curves during humidity absorption and desorption as well as heat-absorbing and releasing processes as shown in Fig. 5 (here, we have only measured the capacitance, instead of both capacitance and resistance, because the sample is same; however, one can also measure the resistance). The hysteresis curve for the humidity sensor is the average value for the total span of humidity.[64] We used the same process for temperature. The average hysteresis for humidity was estimated at 2% with the relative humidity in the range of 0 to 100% RH. For temperature, about 1.5% average hysteresis was estimated in the temperature range of 230 to 310 K. The obtained hysteresis value suggests competency for this sensing device since it is below the threshold of 3%, a maximum value set for a practically competent sensor.[65]

Similarly, the long stability of the graphene-based sensor was checked for humidity and temperature. We checked the stability for one week at room temperature, *i.e.* 295 K and room level relative humidity *i.e.* 36% RH as shown in Fig. 6, where the graphene sensor has shown high stability of both temperature and humidity. However, the stability of the temperature sensor is greater than the stability of the humidity sensor depending on graphene nanoparticles.

3.5. Use of sensors for a steel body

We have used the above sensor on the surface of steel glass to observe the humidity and temperature effect (here, we have only measured the resistance, instead of both capacitance and resistance, because the sample is the same; however, one can also measure the capacitance). This experiment was performed at room temperature of about 22 °C with a relative humidity of about 30% RH. For temperature observation, initially, the glass was empty and the sensor was showing the minimum resistance but as the hot water was poured into the glass, the resistance of the sensor started to increase as shown in Fig. 7.

Similarly, for humidity, the sensor was expressing high resistance. However, as we put the glass in a chamber having about 60% RH, the resistance started to decrease as shown in Fig. 8.

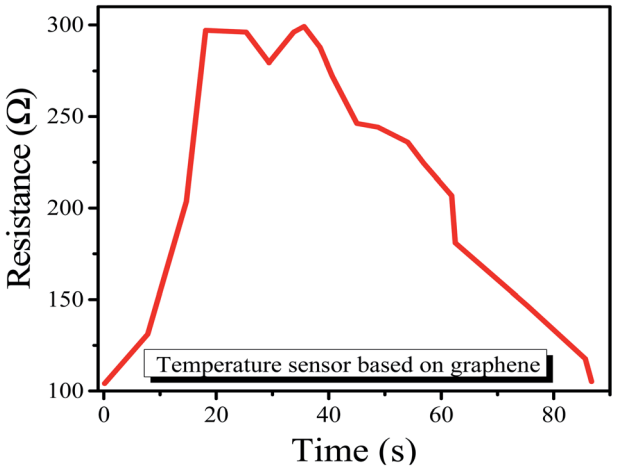

Fig. 7 Resistance output of the temperature sensor.

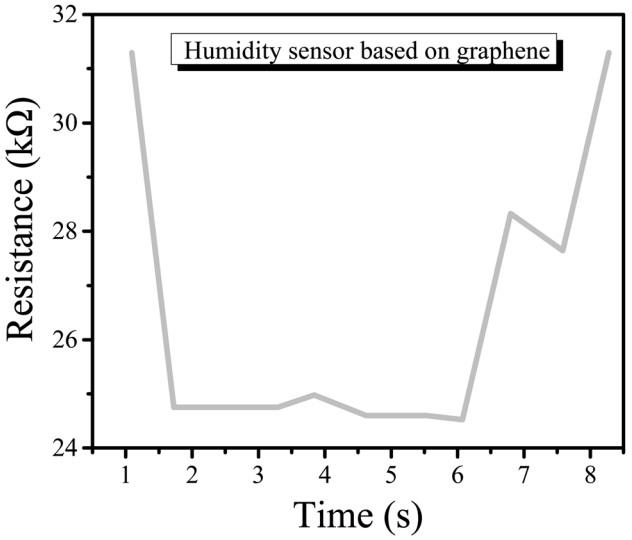

Fig. 8 Resistance output of the temperature sensor.

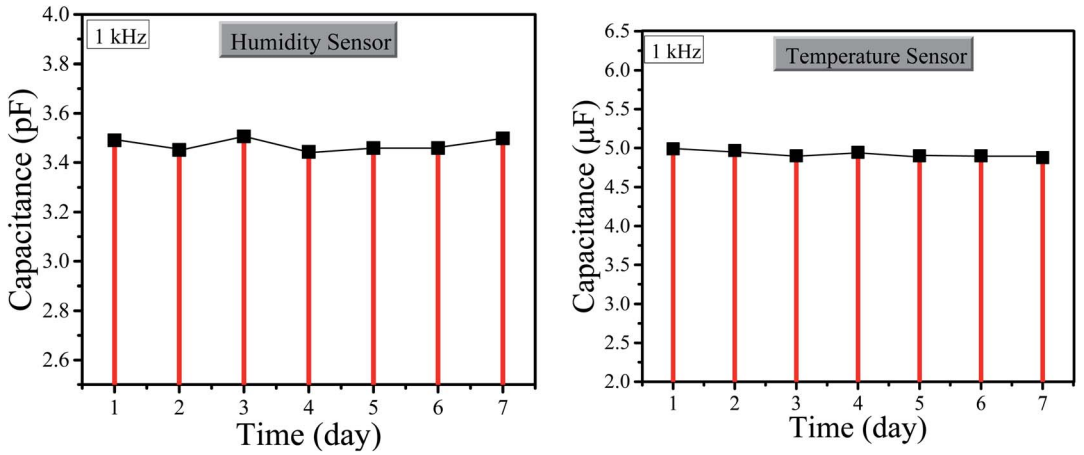

Fig. 6 (Left) Stability graph of the humidity sensor. (Right) Stability graph of the temperature sensor.

3.6. Analysis of capacitance and resistance

It was already mentioned that two types of approaches have been used for the analysis of data, *i.e.*, classical and neutrosophic analysis. For classical analysis, a classical average formula [(maximum value + minimum value)/2] for each interval has been used. Through this, we want to convert interval values into fixed-point values (as classical analysis deals with fixed-point values). However, for neutrosophic analysis, the same interval values (without any modification) have been used by developing a neutrosophic formula for resistance. The measured data of capacitance and resistance are shown in Tables 1 and 2.

3.6.1. Development of the neutrosophic formula. First, we look at the previous definition of the neutrosophic formula. If $Z_N \in [Z_L, Z_U]$ is the random value variable with indeterminacy interval $I_N \in [I_L, I_U]$, then the neutrosophic formula is written as follows:

$$Z_{iN} = Z_{iL} + Z_{iU}I_N \ (i = 1, 2, 3, \ldots n_N) \quad (8)$$

The size of the neutrosophic variable is $n_N \in [n_L, n_U]$. The variable $A_{iN} \in [Z_{iL}, Z_{iU}]$ has two parts: the lower value Z_{iL} is a classical part and the upper value $A_{iU}I_N$ is an indeterminate part having an indeterminacy interval $I_N \in [I_L, I_U]$.

Table 8 Neutrosophic analysis of the measured data of the temperature sensor

Temperature (K)	Capacitance (μF)	Resistance (Ω)
230	$10.01 + 11.12I_N$; $I_N\varepsilon[0, 0.189]$	$90 + 111I_N$; $I_N\varepsilon[0, 0.189]$
240	$10.21 + 10.63I_N$; $I_N\varepsilon[0, 0.041]$	$94 + 98I_N$; $I_N\varepsilon[0, 0.041]$
250	$8.62 + 9.71I_N$; $I_N\varepsilon[0, 0.112]$	$103 + 116I_N$; $I_N\varepsilon[0, 0.112]$
260	$7.52 + 8.55I_N$; $I_N\varepsilon[0, 0.120]$	$117 + 133I_N$; $I_N\varepsilon[0, 0.120]$
270	$6.29 + 7.58I_N$; $I_N\varepsilon[0, 0.170]$	$132 + 159I_N$; $I_N\varepsilon[0, 0.170]$
280	$4.72 + 5.18I_N$; $I_N\varepsilon[0, 0.090]$	$193 + 212I_N$; $I_N\varepsilon[0, 0.090]$
290	$4.02 + 4.49I_N$; $I_N\varepsilon[0, 0.104]$	$223 + 249I_N$; $I_N\varepsilon[0, 0.104]$
300	$3.32 + 3.70I_N$; $I_N\varepsilon[0, 0.103]$	$270 + 301I_N$; $I_N\varepsilon[0, 0.103]$
310	$2.56 + 2.97I_N$; $I_N\varepsilon[0, 0.136]$	$337 + 390I_N$; $I_N\varepsilon[0, 0.136]$

Similarly, the neutrosophic mean $\bar{Z}_N = [\bar{Z}_L, Z_U]$ is defined as follows:

$$\bar{Z}_N = \bar{Z}_L + \bar{Z}_U I_N;\ I_N \in [I_L, I_U] \quad (9)$$

We can use these preliminaries for developing the neutrosophic formula for the present condition. Since the resistance of the graphene nanoparticles depends on the variation of temperature (T) and relative humidity (RH), we can write it as a function of them, *i.e.* $r(T)$ and $r(I)$. The neutrosophic formula for resistance depending on the variance of temperature can be written as follows:

Table 6 Classical analysis of the measured data

Humidity sensor			Temperature sensor		
Relative humidity (% RH)	Capacitance (pF)	Resistance (kΩ)	Temperature (K)	Resistance (Ω)	Capacitance (μF)
0	2.384	36.422	230	100.5	10.061
10	2.597	35.272	240	96	10.421
20	2.894	33.595	250	109.5	9.165
30	3.289	31.408	260	125	8.033
40	3.652	28.582	270	145.5	6.933
50	3.813	26.6845	280	202.5	4.949
60	4.131	24.9225	290	236	4.250
70	4.494	23.5475	300	285.5	3.513
80	4.767	23.203	310	363.5	2.766
90	4.793	23.155			
100	4.897	23.0905			

Table 7 Neutrosophic analysis of the measured data of the humidity sensor

Relative humidity (% RH)	Capacitance (pF)	Resistance (kΩ)
0	$2.345 + 2.923I_N$; $I_N\varepsilon[0, 0.022]$	$36.024 + 36.820I_N$; $I_N\varepsilon[0, 0.012]$
10	$2.421 + 3.213I_N$; $I_N\varepsilon[0, 0.008]$	$35.122 + 35.422I_N$; $I_N\varepsilon[0, 0.012]$
20	$2.710 + 3.312I_N$; $I_N\varepsilon[0, 0.021]$	$33.245 + 33.945I_N$; $I_N\varepsilon[0, 0.012]$
30	$3.001 + 3.299I_N$; $I_N\varepsilon[0, 0.019]$	$31.108 + 31.708I_N$; $I_N\varepsilon[0, 0.006]$
40	$3.398 + 3.663I_N$; $I_N\varepsilon[0, 0.024]$	$28.378 + 28.930I_N$; $I_N\varepsilon[0, 0.006]$
50	$3.419 + 3.824I_N$; $I_N\varepsilon[0, 0.023]$	$26.378 + 26.991I_N$; $I_N\varepsilon[0, 0.006]$
60	$3.721 + 4.143I_N$; $I_N\varepsilon[0, 0.031]$	$24.524 + 25.321I_N$; $I_N\varepsilon[0, 0.006]$
70	$3.921 + 4.521I_N$; $I_N\varepsilon[0, 0.028]$	$23.216 + 23.879I_N$; $I_N\varepsilon[0, 0.012]$
80	$4.007 + 4.791\ I_N$; $I_N\varepsilon[0, 0.007]$	$23.116 + 23.290I_N$; $I_N\varepsilon[0, 0.010]$
90	$4.172 + 4.810I_N$; $I_N\varepsilon[0, 0.006]$	$23.102 + 23.208I_N$; $I_N\varepsilon[0, 0.007]$
100	$4.671 + 4.957I_N$; $I_N\varepsilon[0, 0.001]$	$23.079 + 23.102I_N$; $I_N\varepsilon[0, 0.024]$

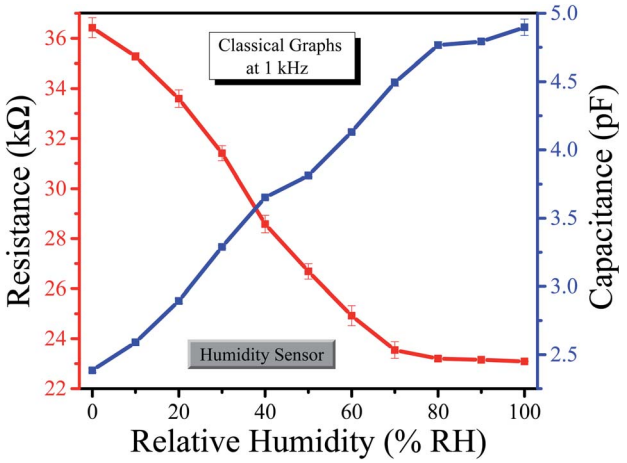

Fig. 9 Classical graph for the humidity sensor.

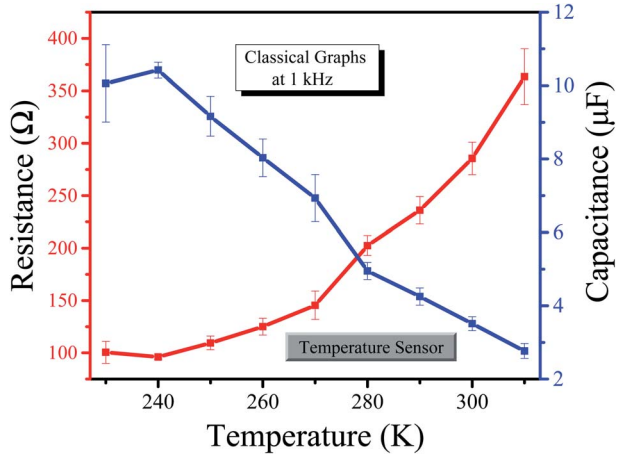

Fig. 10 Classical graph for the temperature sensor.

$$r(T)_N = r(T)_L + r(T)_U I_N;\ I_N \in [I_L, I_U] \quad (10)$$

From the above resistance formula $r(T)_N \in [r(T)_L, r(T)_U]$ is an extension under the classical analysis. The equation contains two parts, *i.e.* $r(T)_L$ determined and $r(T)_U I_N$ indetermined. Moreover, $I_N \in [I_L, I_U]$ is known as an indeterminacy interval. Also, the measured resistance interval $r(T)_N \in [r(T)_L, r(T)_U]$ can be reduced to the classical or determined part if we choose $I_L = 0$ and I_U can be calculated by $(r(T)_U - r(T)_L)/r(T)_U$. Similarly, the neutrosophic formula for capacitance and resistance depending on the variance of relative humidity and temperature can be written as follows:

$$r(\%\ \mathrm{RH})_N = r(\%\ \mathrm{RH})_L + r(\%\ \mathrm{RH})_U I_N;\ I_N \in [I_L, I_U] \quad (11)$$

$$C(\%\ \mathrm{RH})_N = C(\%\ \mathrm{RH})_L + C(\%\ \mathrm{RH})_U I_N;\ I_N \in [I_L, I_U] \quad (12)$$

$$C(T)_N = C(T)_L + C(T)_U I_N;\ I_N \in [I_L, I_U] \quad (13)$$

The classical analysis of the capacitance and the resistance variance with respect to changes in temperature and relative humidity are shown in Table 6. The neutrosophic analysis is shown in Tables 7 and 8 for humidity and temperature, respectively.

The above tables show the classical and neutrosophic analysis of the resistance variance with respect to changes in temperature as well as relative humidity. Classical analysis belongs to or deals with only classical assumptions; this means that the classical approach relates to the classical average value, generally used by researchers in their studies (to avoid complication, we have used this classical average formula as the classical analysis). On the other hand, neutrosophic analysis deals with a novel neutrosophic formula that contains indeterminacy for each measured interval of resistance. We have compared the classical analysis and neutrosophic analysis through graphs for both humidity and temperature sensors. The classical graphs for humidity and temperature are shown in Fig. 9 and 10, respectively.

The neutrosophic graphs for the humidity and temperature sensors are shown in Fig. 11 and 12, respectively.

The graphs above express the comparison between classical analysis and neutrosophic analysis. It can be seen that the graphs of classical analysis are not very flexible because they are drawn at fixed-point values; however, the graphs of the

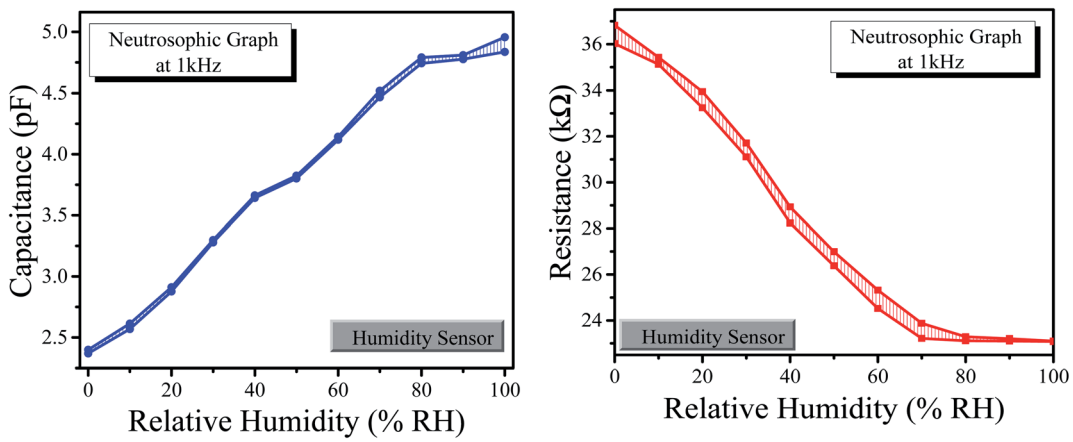

Fig. 11 (Left) Neutrosophic graphs of capacitance for the humidity sensor. (Right) Neutrosophic graphs of resistance for humidity sensor.

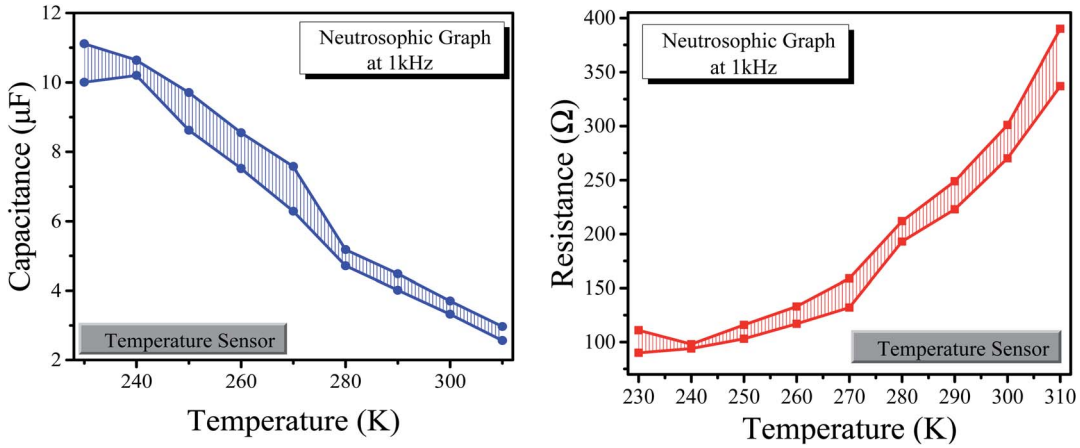

Fig. 12 (Left) Neutrosophic graphs of capacitance for the temperature sensor. (Right) Neutrosophic graphs of resistance for the temperature sensor.

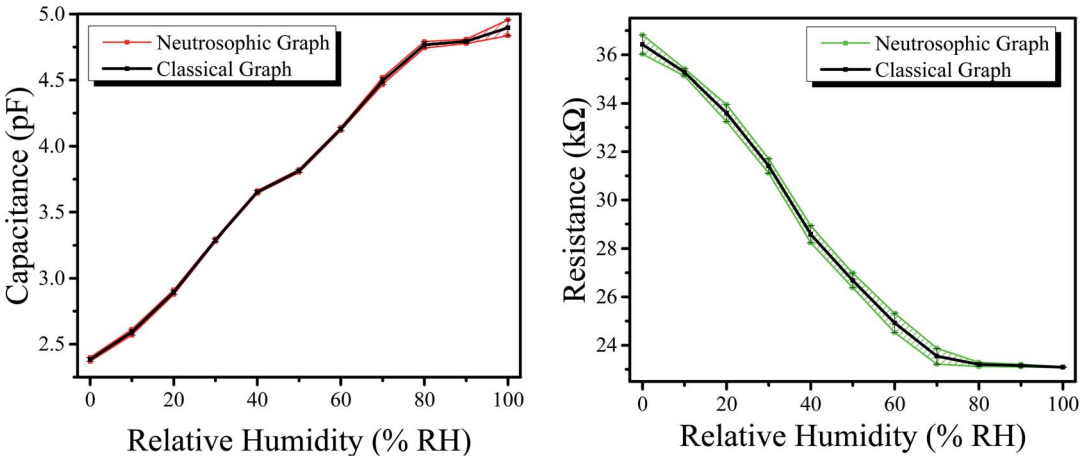

Fig. 13 (Left) Combined graphs of capacitance for the humidity sensor. (Right) Combined graphs of resistance for the humidity sensor.

neutrosophic analysis show more flexibility. Also, one can observe the classical graphs through neutrosophic graphs as these are at the center of neutrosophic graphs (which shows that the neutrosophic analysis is a generalization of classical graphs) as shown in the combined graphs of Fig. 13 and 14. This means that neutrosophic statistics are more effective for

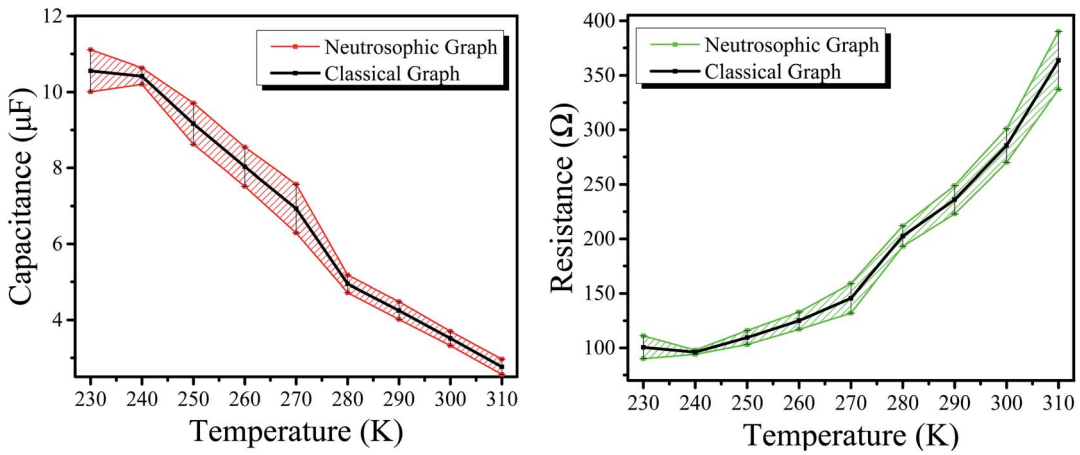

Fig. 14 (Left) Combined graphs of capacitance for the temperature sensor. (Right) Combined graphs of resistance for the temperature sensor.

analyzing the resistance of the sample.[66] As a result, the neutrosophic analysis is more informative, flexible and adequate than the classical analysis.

4. Conclusion

This work is based on the fabrication of a graphene nanoparticle thin-film-based sensor for the detection of humidity and temperature on a metal body. A thin film of graphene nanoparticles was deposited between two silver electrodes on a clean glass substrate. The structural properties of the thin film were studied *via* XRD, the quality was investigated *via* Raman spectroscopy and optical properties by UV-vis. The electric properties (capacitance and resistance) of the sample with respect to relative humidity (% RH) and temperature (K) were determined separately using an LCR meter in a controlled chamber. The graphene sensor expressed good sensitivity with fast response and recovery times, *i.e.* 1.6 s and 2.15 s for the humidity and 3 s and 8.1 s for the temperature, respectively. It also expressed long stability for both humidity and temperature and low average hysteresis, *i.e.* 2% for humidity and 1.5% for temperature. The classical and neutrosophic analyses of the capacitance and resistance were performed *via* the application of material statistics, and it was found that neutrosophic analysis is more informative and flexible for explaining the capacitance and resistance of the sensors.

Conflicts of interest

There are no conflicts to declare.

References

1 M. Dimchev, R. Caeti and N. Gupta, Effect of carbon nanofibers on tensile and compressive characteristics of hollow particle filled composites, *Mater. Des.*, 2010, **31**(3), 1332–1337.
2 Z. Zhang, *et al.*, Fabrication and characterization of closed-cell aluminum foams with different contents of multi-walled carbon nanotubes, *Mater. Des.*, 2015, **88**, 359–365.
3 U. Afzal, *et al.*, Fabrication of flexible temperature sensors to explore indeterministic data analysis for robots as an application of Internet of Things, *RSC Adv.*, 2022, **12**, 17138–17145.
4 A. K. Geim and K. S. Novoselov, The rise of graphene, in *Nanoscience and technology: a collection of reviews from nature journals*, World Scientific, 2010, pp. 11–19.
5 C. Lee, *et al.*, Measurement of the elastic properties and intrinsic strength of monolayer graphene, *Science*, 2008, **321**(5887), 385–388.
6 J.-W. Jiang, J.-S. Wang and B. Li, Thermal conductance of graphene and dimerite, *PPhys. Rev. B: Condens. Matter Mater. Phys.*, 2009, **79**(20), 205418.
7 J.-H. Chen, *et al.*, Intrinsic and extrinsic performance limits of graphene devices on SiO_2, *Nat. Nanotechnol.*, 2008, **3**(4), 206–209.
8 A. K. Geim, Graphene: status and prospects, *Science*, 2009, **324**(5934), 1530–1534.
9 N. Zaaba, *et al.*, Synthesis of graphene oxide using modified hummers method: solvent influence, *Procedia Eng.*, 2017, **184**, 469–477.
10 N. Cao and Y. Zhang, Study of reduced graphene oxide preparation by Hummers' method and related characterization, *J. Nanomater.*, 2015, **2015**, 168125.
11 Y. Hou, *et al.*, High-quality preparation of graphene oxide via the Hummers' method: understanding the roles of the intercalator, oxidant, and graphite particle size, *Ceram. Int.*, 2020, **46**(2), 2392–2402.
12 S. N. Alam, N. Sharma and L. Kumar, Synthesis of graphene oxide (GO) by modified hummers method and its thermal reduction to obtain reduced graphene oxide (rGO), *Graphene*, 2017, **6**(1), 1–18.
13 E. W. Hill, A. Vijayaragahvan and K. Novoselov, Graphene sensors, *IEEE Sens. J.*, 2011, **11**(12), 3161–3170.
14 D. H. Shin and S.-H. Choi, Use of graphene for solar cells, *J. Korean Phys. Soc.*, 2018, **72**(12), 1442–1453.
15 D.-T. Phan and G.-S. Chung, Effects of rapid thermal annealing on humidity sensor based on graphene oxide thin films, *Sens. Actuators, B*, 2015, **220**, 1050–1055.
16 X. Li, *et al.*, High-sensitive humidity sensor based on graphene oxide with evenly dispersed multiwalled carbon nanotubes, *Mater. Chem. Phys.*, 2018, **207**, 135–140.
17 J. Yang, *et al.*, Wearable temperature sensor based on graphene nanowalls, *RSC Adv.*, 2015, **5**(32), 25609–25615.
18 N. Dong, *et al.*, Pressure and temperature sensor based on graphene diaphragm and fiber Bragg gratings, *IEEE Photonics Technol. Lett.*, 2017, **30**(5), 431–434.
19 Y. Wang, *et al.*, High-sensitivity wearable and flexible humidity sensor based on graphene oxide/non-woven fabric for respiration monitoring, *Langmuir*, 2020, **36**(32), 9443–9448.
20 M. Hilal and J. I. Han, Development of a highly flexible and durable fiber-shaped temperature sensor based on graphene/Ni double-decked layer for wearable devices, *IEEE Sens. J.*, 2020, **20**(10), 5146–5154.
21 M. Soni, *et al.*, Printed temperature sensor based on PEDOT:PSS-graphene oxide composite, *IEEE Sens. J.*, 2020, **20**(14), 7525–7531.
22 Z. Chen, *et al.*, Flexible temperature sensors based on carbon nanomaterials, *J. Mater. Chem. B*, 2021, **9**(8), 1941–1964.
23 D. Wang, *et al.*, Electrospinning of flexible poly(vinyl alcohol)/MXene nanofiber-based humidity sensor self-powered by monolayer molybdenum diselenide piezoelectric nanogenerator, *Nano-Micro Lett.*, 2021, **13**(1), 1–13.
24 L. Zhang, *et al.*, Triboelectric nanogenerator based on Teflon/vitamin B1 powder for self-powered humidity sensing, *Beilstein J. Nanotechnol.*, 2020, **11**(1), 1394–1401.
25 X. Liu, *et al.*, A humidity sensing and respiratory monitoring system constructed from quartz crystal microbalance sensors based on a chitosan/polypyrrole composite film, *J. Mater. Chem. A*, 2021, **9**(25), 14524–14533.

26 D. Wang, *et al.*, Multifunctional latex/polytetrafluoroethylene-based triboelectric nanogenerator for self-powered organ-like MXene/metal–organic framework-derived CuO nanohybrid ammonia sensor, *ACS Nano*, 2021, **15**(2), 2911–2919.
27 F. Smarandache, *Introduction to neutrosophic measure, neutrosophic integral, and neutrosophic probability*, Infinite Study, 2013.
28 M. Aslam, A study on skewness and kurtosis estimators of wind speed distribution under indeterminacy, *Theor. Appl. Climatol.*, 2021, **143**(3), 1227–1234.
29 J. Ye, Improved cosine similarity measures of simplified neutrosophic sets for medical diagnoses, *Artif. Intell. Med.*, 2015, **63**(3), 171–179.
30 V. Christianto, R. N. Boyd and F. Smarandache, *Three possible applications of neutrosophic logic in fundamental and applied sciences*, Infinite Study, 2020.
31 M. Aslam, Enhanced statistical tests under indeterminacy with application to earth speed data, *Earth Sci. Inform.*, 2021, 1–7.
32 U. Afzal, *et al.*, Neutrosophic statistical analysis of resistance depending on the temperature variance of conducting material, *Sci. Rep.*, 2021, **11**(1), 1–6.
33 U. Afzal, M. Aslam and A. H. Al-Marshadi, Analyzing imprecise graphene foam resistance data, *Mater. Res. Express*, 2022, **9**, 045007.
34 F. Smarandache, *The Neutrosophic Research Method in Scientific and Humanistic Fields*, 2010.
35 F. Smarandache, *Introduction to neutrosophic statistics: Infinite Study*, Romania-Educational Publisher, Columbus, OH, USA, 2014.
36 J. Chen, J. Ye and S. Du, Scale effect and anisotropy analyzed for neutrosophic numbers of rock joint roughness coefficient based on neutrosophic statistics, *Symmetry*, 2017, **9**(10), 208.
37 J. Chen, *et al.*, Expressions of rock joint roughness coefficient using neutrosophic interval statistical numbers, *Symmetry*, 2017, **9**(7), 123.
38 M. Aslam, Design of the Bartlett and Hartley tests for homogeneity of variances under indeterminacy environment, *J. Taibah Univ. Sci.*, 2020, **14**(1), 6–10.
39 M. Aslam, On detecting outliers in complex data using Dixon's test under neutrosophic statistics, *J. King Saud Univ., Sci.*, 2020, **32**(3), 2005–2008.
40 U. Afzal, *et al.*, Fabrication of a surface type humidity sensor based on methyl green thin film, with the analysis of capacitance and resistance through neutrosophic statistics, *RSC Adv.*, 2021, **11**(61), 38674–38682.
41 G. Yang, *et al.*, Structure of graphene and its disorders: a review, *Sci. Technol. Adv. Mater.*, 2018, **19**(1), 613–648.
42 A. C. Ferrari, *et al.*, Raman spectrum of graphene and graphene layers, *Phys. Rev. Lett.*, 2006, **97**(18), 187401.
43 B. Qin, *et al.*, Crystalline Molybdenum Carbide–Amorphous Molybdenum Oxide Heterostructures: In Situ Surface Reconfiguration and Electronic States Modulation for Li–S Batteries, *Energy Storage Materials*, 2022, 14752.
44 C.-L. Dai, A capacitive humidity sensor integrated with micro heater and ring oscillator circuit fabricated by CMOS–MEMS technique, *Sens. Actuators, B*, 2007, **122**(2), 375–380.
45 R. M. Metzger, *Unimolecular and Supramolecular Electronics I: Chemistry and Physics Meet at Metal-Molecule Interfaces*, Springer Science & Business Media, vol. 312, 2012.
46 J. Korvink, *et al.*, Accurate 3D capacitance evaluation in integrated capacitive humidity sensors, *Sens. Mater.*, 1993, **4**, 323.
47 M. Matsuguchi, *et al.*, Characterization of polymers for a capacitive-type humidity sensor based on water sorption behavior, *Sens. Actuators, B*, 1998, **49**(3), 179–185.
48 M. A. Omar, *Elementary solid state physics: principles and applications*, Pearson Education India, 1975.
49 M. Tahir, *et al.*, Humidity, light and temperature dependent characteristics of Au/N-BuHHPDI/Au surface type multifunctional sensor, *Sens. Actuators, B*, 2014, **192**, 565–571.
50 M. Shah, *et al.*, Carbon nanotubes' nanocomposite in humidity sensors, *Solid-State Electron.*, 2012, **69**, 18–21.
51 P. Li, *et al.*, Humidity sensor based on electrospun (Na0. 5Bi0. 5) 0.94 TiO3–Ba0. 06TiO3 nanofibers, *Ceram. Int.*, 2015, **41**(10), 14251–14257.
52 N. M. Kiasari, *et al.*, Room temperature ultra-sensitive resistive humidity sensor based on single zinc oxide nanowire, *Sens. Actuators, A*, 2012, **182**, 101–105.
53 M. Haditale, R. Dariani and E. Ghasemian Lemraski, Electrical behavior of graphene under temperature effect and survey of I–T curve, *J. Theor. Appl. Phys.*, 2019, **13**(4), 351–356.
54 E. Gibney, Graphene conducts electricity ten times better than expected, *Nature*, 2014, **2**(6), 2–4.
55 M. Dewapriya, A. S. Phani and R. Rajapakse, Influence of temperature and free edges on the mechanical properties of graphene, *Modell. Simul. Mater. Sci. Eng.*, 2013, **21**(6), 065017.
56 C. Wang, *et al.*, Metal oxide gas sensors: sensitivity and influencing factors, *Sensors*, 2010, **10**(3), 2088–2106.
57 Q. Kuang, *et al.*, High-sensitivity humidity sensor based on a single SnO2 nanowire, *J. Am. Chem. Soc.*, 2007, **129**(19), 6070–6071.
58 W.-P. Chen, *et al.*, A capacitive humidity sensor based on multi-wall carbon nanotubes (MWCNTs), *Sensors*, 2009, **9**(9), 7431–7444.
59 Z. Ahmad, *et al.*, Humidity-dependent characteristics of methyl-red thin film-based Ag/methyl-red/Ag surface-type cell, *Phys. E*, 2008, **41**(1), 18–22.
60 V. S. Turkani, *et al.*, A carbon nanotube based NTC thermistor using additive print manufacturing processes, *Sens. Actuators, A*, 2018, **279**, 1–9.
61 J.-S. Kim, K.-Y. Chun and C.-S. Han, Ion channel-based flexible temperature sensor with humidity insensitivity, *Sens. Actuators, A*, 2018, **271**, 139–145.
62 Q. Liu, *et al.*, A high-performances flexible temperature sensor composed of polyethyleneimine/reduced graphene oxide bilayer for real-time monitoring, *Adv. Mater. Technol.*, 2019, **4**(3), 1800594.

63 N. Neella, *et al.*, Scalable fabrication of highly sensitive flexible temperature sensors based on silver nanoparticles coated reduced graphene oxide nanocomposite thin films, *Sens. Actuators, A*, 2017, **268**, 173–182.
64 M. I. Azmer, *et al.*, Humidity sensor based on electrospun MEH-PPV: PVP microstructured composite, *RSC Adv.*, 2016, **6**(42), 35387–35393.
65 M. Ueda, *et al.*, Water-resistant humidity sensors based on sulfonated polyimides, *Sens. Actuators, B*, 2007, **127**(2), 463–470.
66 U. Afzal, J. Afzal and M. Aslam, Analyzing the Imprecise Capacitance and Resistance Data of Humidity Sensors, *Sens. Actuators, B*, 2022, 132092.